

Retinal Vessel Segmentation from Fundus Images

Michael Sandborn, James Raubenheimer

CS8395 - Fall 2020 - Dr. Oguz

Abstract. Segmentation of retinal fundus images allows for early detection and treatment of eye disease such as diabetic retinopathy and macular degeneration. However, the variation in structure and orientation of features within the eye such as retinal blood vessels and the optic nerve head make it difficult to generalize this process. We explore pre-processing including intensity rescaling and thresholding, and use the pre-processed images as input to a random walk segmentation task. Performance is measured with Dice scores, and the fractal dimension as a marker for retinal disease is investigated.

1 Introduction

Segmentation of retinal fundus images is an important step in characterising a variety of eye diseases. Structures such as the optic cup, optic disc, and retinal blood vessels provide early indicators of diseases such as glaucoma, cataract, diabetic retinopathy, and age-related macular degeneration (AMD), all of which may cause irreversible blindness [1]. However, retinal fundus images can be difficult to segment for a few reasons: the heterogeneity of vessel size and structure, and intensity variation across the image and between vessels makes thresholding difficult. **Related Work.** A variety of techniques have been proposed for the segmentation of retinal blood vessels, including random walk segmentation, vessel importance methods [3], and graph cut variants [6]. Recently, various deep learning approaches with U-Net architecture have shown promise with very high accuracy in segmenting fundus images compared to ground truth labels produced manually. Retinal fundus images capture the inside back surface of the eye using a camera that points through the pupil. This type of image captures the retina, macula, optic disc, fovea, and blood vessels [7]. These structures indicate features or abnormalities useful for diagnosing diseases of the eye, e.g. cup-to-disc ratio for detection of glaucoma [9], neovascularization from hemorrhage, or presence of exudates around vessels for early indication of diabetic retinopathy [10]. These features can be detected with effective segmentation methods. However, the severity of these features and similar characteristics as well as general anatomical variation make it difficult to develop a robust and effective segmentation method. In this work, we focus on the pre-processing of fundus images and the segmentation of retinal blood vessels. We assess the performance of a random walk segmentation after pre-processing with Gaussian smoothing, intensity

rescaling, and Hessian image extraction. We use Dice scores and fractal dimension to compare the random walk results with the ground truth segmentations provided with the data.

1.1 Data & Tools

We use data from the DRIVE [5] and STARE [15] datasets containing normal and abnormal retinal fundus images as well as manual ground truth segmentations. The DRIVE dataset comes from a diabetic retinopathy screening program in the Netherlands and contains fundus images from subjects between 25-90 years of age. Of the 40 total images, 33 are normal and 7 exhibit diabetic retinopathy at various stages. We only use 20 of these images and their ground truth segmentations from DRIVE, as the other 20 images do not contain the ground truth segmentation as advertised. The STARE project contains approximately 400 color fundus images including 20 manual segmentations. Of the 20 labeled images, 7 are normal and 13 exhibit a variety of eye disease including neovascularization, drusen, vein occlusion, diabetic retinopathy, and macroaneurysm. To conduct the study, we use ITK Python for pre-processing methods, scikit-image for random walk segmentation and post-processing, and Slicer for visualization.

1.2 Overview

We investigate whether a Hessian image with multi-level smoothing is a viable pre-processing step for retinal vessel segmentation with the random walk algorithm. We evaluate our segmentation results with the Dice score and also assess the viability of the fractal dimension in helping to classify normal vs. abnormal fundus images.

1.3 Hypothesis

We hypothesize that the random walk segmentation on the Hessian image with intensity rescaling may rival automated segmentation results or provide a competitive baseline to be further adjusted by automated methods. Additionally, the fractal dimension should supplement other metrics of retinal structures (e.g. cup-to-disc ratio) to improve accuracy of downstream automated classification.

1.4 Evaluation Metrics

We use Dice scores to compare the results of the random walk segmentation from the Hessian image with the ground truth segmentation. We also provide the fractal dimensions of the ground truth segmentation to compare with the random walk segmentation. The fractal dimension of an image has been explored as a potential biomarker for diabetic retinopathy detection in particular [16].

1.5 Division of Work

Michael contributes the pre-processing steps as well as the fractal dimension values and analysis; **James** provides the initial data setup and the random walk segmentation and dice scores.

2 Pre-processing

We begin by experimenting with pre-processing steps for a retinal fundus image. Using ITK filters, we obtain the grayscale image from the color image before experimenting with feature visibility enhancement. **Smoothing** Gaussian smoothing is applied with ITK's SmoothingRecursiveGaussianImageFilter and $\sigma = 1, 2, 4$ to capture the variety of vessel size structure (e.g. thin and hair-like vs. large and tubular) and produce 3 smoothed feature images added together to enhance clarity of vessels of different sizes. We also experiment with $\sigma = (1, 3, 5), (2, 4, 6)$. The approach of adding smoothed images for different sized features does not generalize well to a population of fundus images as shown in Figure 3. In particular, the presence of eye disease introduces noise when adding and smoothing. The variation and heterogeneity in feature size, structure, and location also makes it difficult to establish a robust smoothing procedure for a set of images. The average of the three smoothed images was also extracted but produced a similar issue. **Thresholding** To alleviate this, we experimented with window thresholding around vessels as well as intensity scaling to focus the features of interest (vessels, optic nerve head) using IntensityWindowingImageFilter and RescaleIntensityImageFilter, respectively, but this also resulted in unwanted noise and interference around these areas. A possible explanation for this is the glossy nature of fundus images which cause large intensity differences in small neighboring regions around ROIs, making it difficult to effectively threshold to a single value in a specific region of the image. We also try both window thresholding and traditional thresholding as shown in figure with intensity ranges between approximately 25-80 after intensity rescaling for vessel detection. Another issue with this approach is the "vanishing vessel" problem: as the branches of the superior and inferior temporal archade converge towards the macula region, the intensities of these very thin vessels approach the intensities of the immediate surroundings and the vessels are not detected by the threshold range (including the vessel's intensity value in the target threshold range would then cause the surrounding area to cover the vessel because of this similarity) thus this approach is also complicated by a range of pixel intensities as well as intensity blending near vessel boundaries. While intensity rescaling helps maintain visibility of smaller vessels, thresholding the entirety a population of fundus images with a single threshold approach remains a difficult task. We also experiment with ITK's IsolatedConnectedImageFilter to try to automate thresholding by setting seeds at explicit locations on the image as well as defining a replacement intensity value to set on either side of the threshold calculated by the filter. The intuition for this approach was to set seed coordinates at the top and bottom of the manually located optic nerve head and set a replacement

value to capture the vessels rooted at the optic nerve head, the main superior and inferior temporal archades and the vessels branching from them in the top and bottom halves of the eye, respectively. This approach also suffers from intensity variation as the results of this filter creates large blotches of a single intensity value which either covered the vessels or did not detect them at all.

Hessian Filtering To address the issues with general thresholding and smoothing of retinal images with disease, we apply a Hessian-based filtering approach for identifying structures in the retinal image and avoiding the issues associated with the complexity of accommodating intensity scales of many fundus images. The Hessian matrix \mathbf{H} of a function $f : R^n \rightarrow R$ is the Jacobian matrix of the gradient which is the matrix containing all second-order partial derivatives of the intensity values of an image. The Hessian matrix is useful for identifying structures based on local image intensities by obtaining the eigenvalues of the image. The relative values of the n eigenvalues are categorized (e.g low, high positive, and high negative). General structures are then identified using a table of these eigenvalue arrangements: sheets, blobs, and tubes are detectable in addition to brightness or darkness [11]. To detect vessel structures, we use the HessianToObjectnessMeasureImageFilter combined with the MultiScaleHessian-BasedMeasureImageFilter in ITK. The first of these takes an image of Hessian pixels and produces an enhanced image containing a certain structure, vessels in this case. The required parameters for this filter are the following: SetBrightObject, SetScaleObjectnessMeasure, and values for α, β, γ . SetBrightObject is a boolean indicating whether to enhance bright structures on a dark background. This was set to false since the grayscale vessels appear darker than the surroundings. SetScaleObjectnessMeasure is a boolean indicating whether to scale "objectness" with the magnitude of the largest eigenvalue. This was set to true. The parameters α, β control the weights of the ratios between different sized eigenvalues with smaller values causing increased sensitivity to image dimensionality. After experimenting with $\alpha, \beta = (1.0, 1.0), (0.7, 0.7), (0.7, 0.5)$, we set $\alpha, \beta = (0.5, 0.5)$ for the most detail and clarity and least background interference. The MultiScaleHessianBasedMeasureImageFilter computes the grayscale image of the identified structure using the configured HessianToObjectnessMeasureImageFilter after internally calculating the Hessian images with ITK's HessianRecursiveGaussianImageFilter [12]. For the input to this filter, we used the initial approach of the Gaussian smoothing filter at 3 levels: $\sigma = 1, 2, 4$. This has the benefit of enhancing both the contrast and sharpness of the different size vessels of the image as well as removing the intensity variation problem across non-vessel regions since the Hessian filter detects tubular structures. The final output of this filter is the best response of the Hessian matrix to the Hessian measure filter at all of the scales, given by SetNumberOfSigmaSteps which we left at the default of 10. We also left the other parameters for this filter, SetSigmaMinimum and SetSigmaMaximum at the default values of 1 and 2, respectively. Figure 4 shows some of the calculated Hessian images from this approach. The Gaussian smoothed image combined with the Hessian filter as pre-processing steps eliminate the issues outlined above with thresholding and feature detection by

intensity ranges or explicit regions of the fundus image. While the Hessian filter provides a structural baseline for the set of fundus images, it still does not capture the entirety of the vessel network. For this reason, we use the Hessian image as initial input to a random walk segmentation pipeline which performs a random walk on the Hessian image plus thresholding and small object removal as post-processing steps. The final image is then compared with the ground truth segmentation with Dice scores and fractal dimension values.

Fig. 1. 3 fundus images - STARE 005 (abnormal- central retinal artery occlusion), DRIVE 01 (normal), DRIVE 26 (abnormal- background diabetic retinopathy)



Fig. 2. Grayscale images

3 Random Walk Segmentation

The random walker algorithm for segmentation produces a segmentation based on pre-defined seed points and calculates probabilities for all unlabeled pixels randomly walking across the image. The label associated with the label of maximum probability to be reached by a walker of a given pixel is the label assigned to the pixel [17].



Fig. 3. Added smoothed features for normal fundus image (center) vs. abnormal

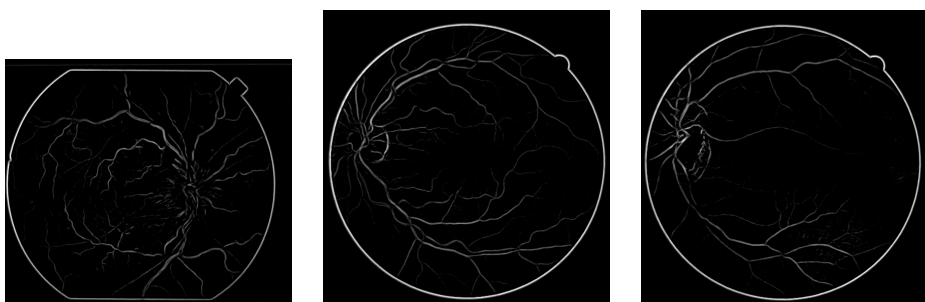


Fig. 4. Hessian images

3.1 Setup

For our approach, we use the smoothed Hessian image of the fundus image as input and process the image with the following steps: using sci-kit image, the Hessian image is read in as a gray image and intensity is rescaled from grayscale to $[-1, 1]$. After rescaling, the markers for the random walk segmentation are then set according to intensity cutoffs of $-.98$ and $.98$ from the rescaled Hessian image. If a pixel value lies below $-.98$, we assign it to seed group 1; if it lies above $.98$ we assign it to seed group 2. These markers are stored in an array representing the seed group for each pixel. The sci-kit image random_walker function returns an array of labels according to the method described above. These labels are then post-processed in the following manner to obtain the final segmentation from the labels: the label image is inverted to match the coloring of the segmentation (white vessels on black background) and then a bilateral denoising filter is applied using sci-kit image's denoise_bilateral function. We apply Otsu thresholding [18] to obtain the upper threshold of the image and binarize the denoised segmentation according to each pixel value compared to the upper threshold value. Finally, we remove small islands from the image using remove_small_objects specifying a parameter of min_size to denote the minimum allowable size, in pixels, of objects to remain in the image.

3.2 Results

Table 1. Description and Dice scores for the 10 images in the figures below: **H** is the input Hessian image, **S** is the ground truth segmentation, **R** is the random walk segmentation, **DR** is diabetic retinopathy; **H-S** indicates the Dice score between the input Hessian image and the ground truth segmentation.

ImageID	H-S	H-R	S-R	Diagnosis	Dataset
011	.517	.614	.766	Normal	DRIVE
004	.548	.637	.764	Normal	DRIVE
236	.579	.698	.759	Normal	STARE
014	.480	.604	.745	DR	DRIVE
017	.511	.606	.743	DR	DRIVE
003	.511	.579	.735	DR	DRIVE
139	.501	.657	.691	DR	STARE
239	.517	.641	.685	Normal	STARE
240	.552	.667	.623	Normal	STARE
001	.422	.667	.521	DR	STARE

3.3 Analysis

Dice scores for fundus images with normal diagnosis were greater than for those with abnormal diagnosis. We focus particularly on diabetic retinopathy in

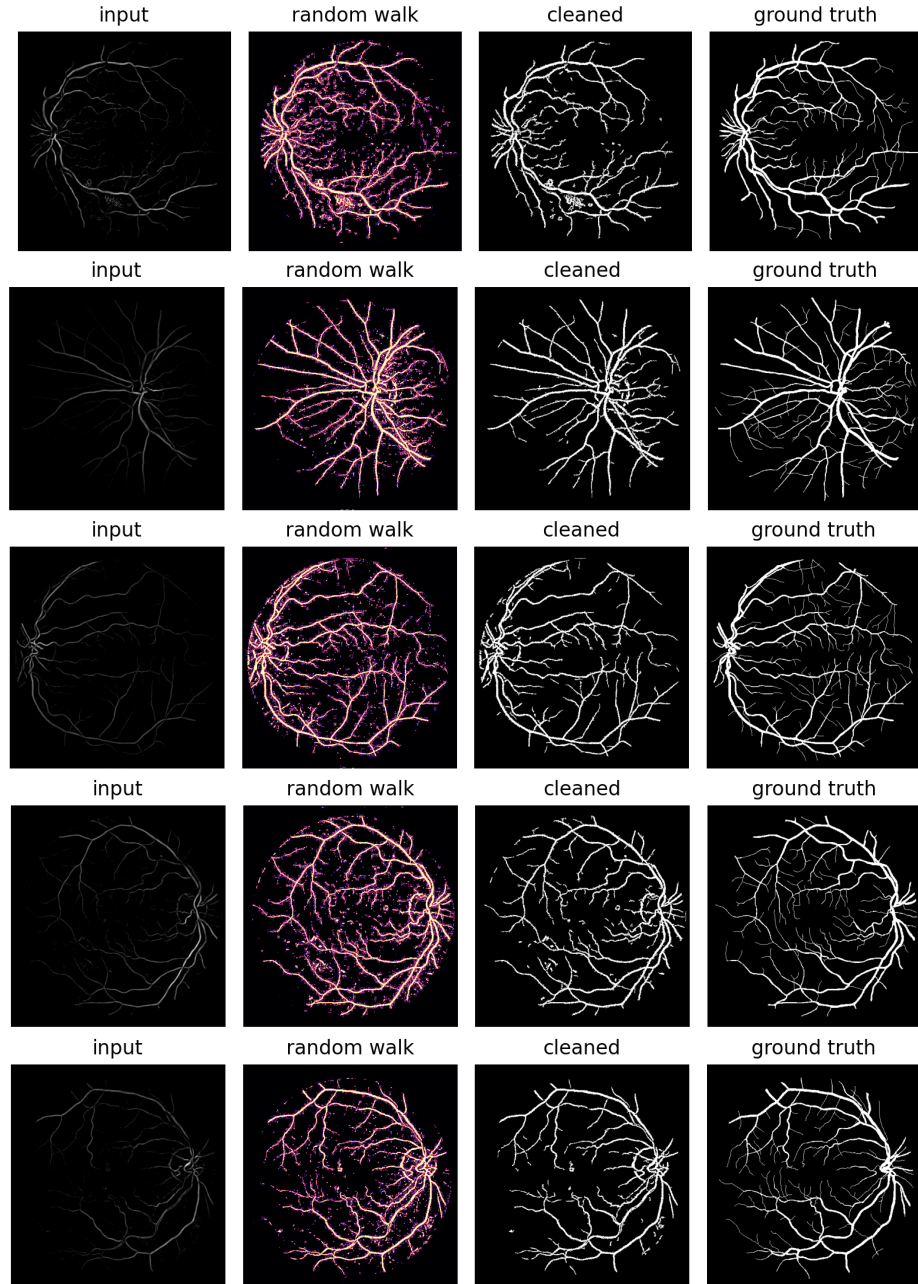


Fig. 5. Random walk segmentation for DRIVE images - 03,04,11,14,17

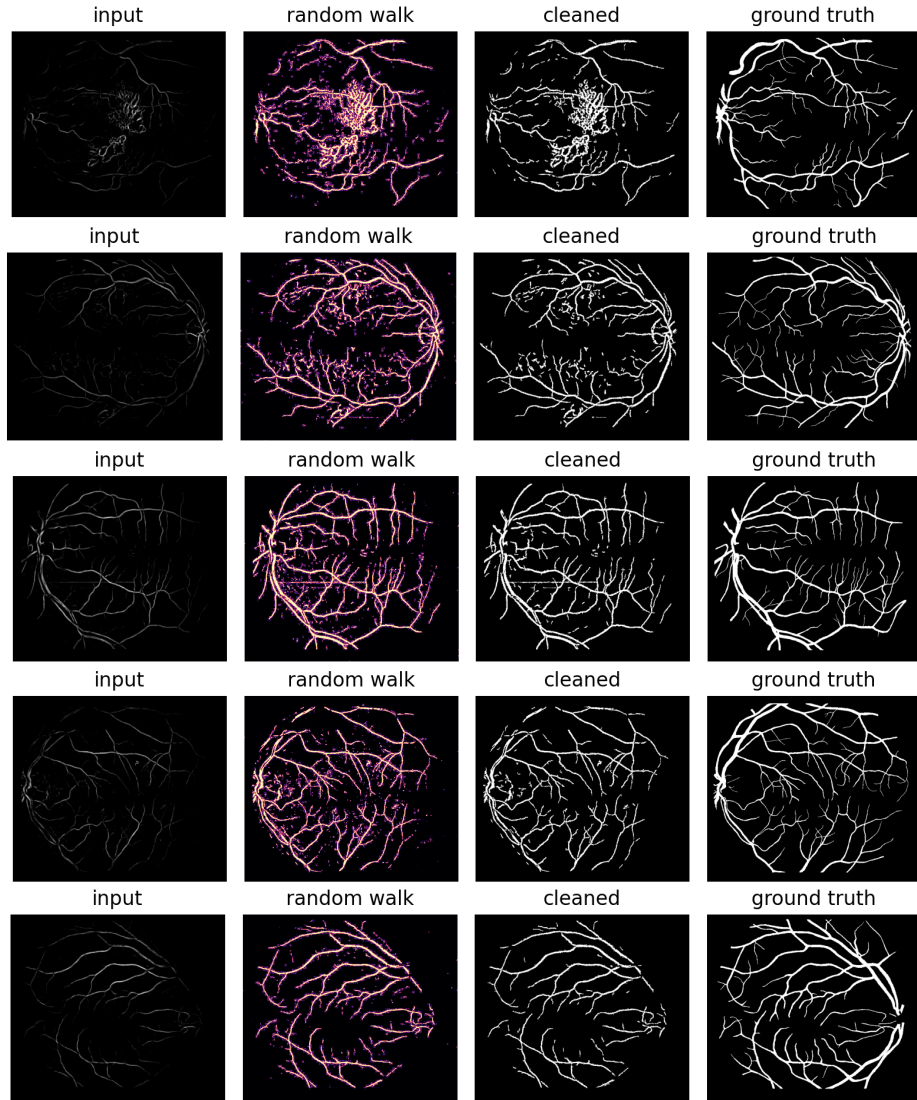


Fig. 6. Random walk segmentation for STARE images - 001,139,236,239,240

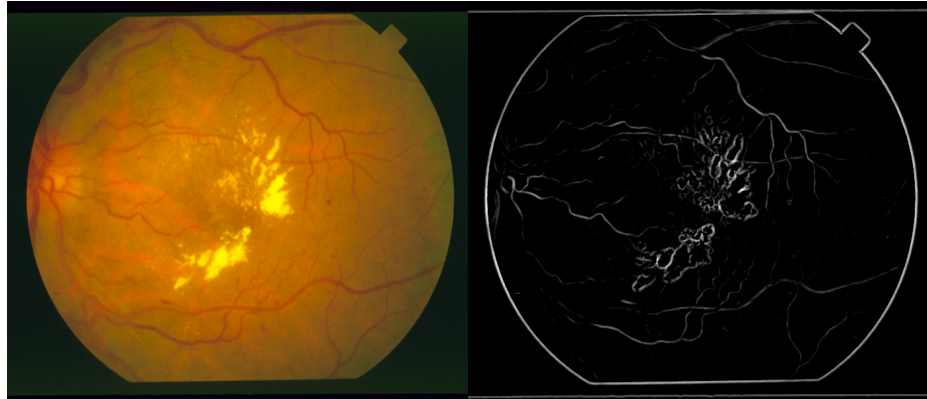


Fig. 7. STARE 001 (abnormal- diabetic retinopathy) and its Hessian image

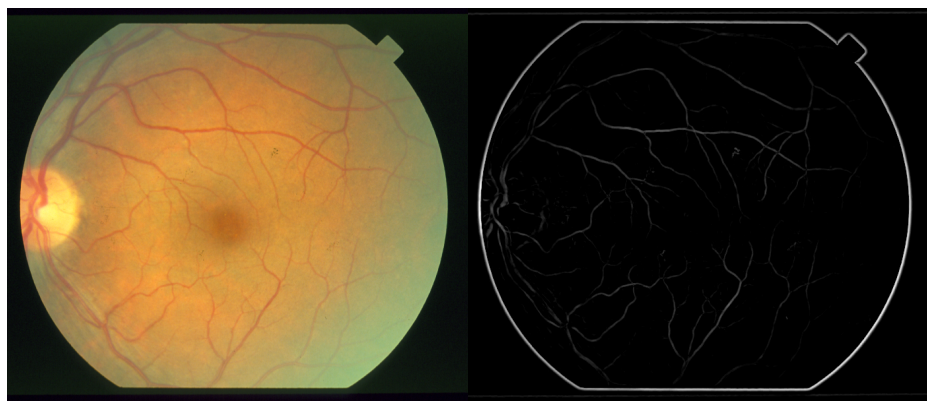


Fig. 8. STARE 239 (normal) and its Hessian image

this analysis since it's a progressive disease of the eye with symptoms manifesting over time. For images with diabetic retinopathy, the Hessian image captures features of the eye disease around the vessels in addition to the vessels themselves, resulting in a hazy Hessian image with blurry loop-like structures that partially occlude the vessels as shown in Figure 7. Figures 3 and 4 show the white halo around the resulting images which was an issue when comparing the dice scores of the random walk result with the ground truth. The halo originates from the input Hessian image which is extracted from the added smoothed features of the original grayscale image. With each additional image, the clarity of vessels is enhanced but the halo (edge of the fundus image on background) thickens. As mentioned before, taking the average of the added smoothed images did not alleviate the halo problem. After attempts with thresholding and erosion to remove the halos, these were ultimately removed manually because the vessels were connected to the halo in various regions in the image depending on the orientation and presence of disease of the vessels. Without the halo around the images, the Dice scores between the random walk result and the ground truth increased by $\approx .1$ for each of the images.

4 Fractal dimension as a metric for disease classification

The fractal dimension as a potential biomarker for disease has been explored for structures containing vessel-like features [16]. The fractal dimension, fd , is given by the formula

$$fd = \frac{\log N(r)}{\log r} \quad (1)$$

Where $N(r)$ is a measurement taken on an object with local self-similarity properties and r is some scale at which these measurements are taken [16]. In this work, we provide an implementation of this equation according to the box counting method, where a binary image is covered with a set of uniform boxes of decreasing size and increasing quantity. In each of the boxes covering an image region, the presence of a target pixel value which represents self-similarity detail [19] is determined. The value fd is then calculated from the ratio of the log of $N(r)$ and r , the number of boxes containing self-similarity detail at each scale over a range of scales. In this case, where multiple scales are considered, fd represents the slope of the line containing the box count as a function of the scale (ordered pairs of $(r, N(r))$).

4.1 Setup

For this task, we use the ground truth segmentation of the 40 total images provided by DRIVE and STARE as well as the diagnosis codes indicating either normal or abnormal with a description of the eye disease. Each ground truth segmentation is inverted for enhanced visibility, and the box counting algorithm is run on each of the images. The calculated fractal dimension and the

corresponding diagnosis for 7 of the 40 images are listed below. We also include the fractal dimension calculated from the random walk segmentation results for comparison.

4.2 Results

Table 2. Fractal dimension values and diagnoses for 7 images from DRIVE and STARE

ImageID	fd , ground truth	fd , random walk	Diagnosis	Dataset
03	1.734	1.685	DR	DRIVE
04	1.746	1.682	Normal	DRIVE
001	1.733	1.723	DR	STARE
139	1.755	1.759	DR	STARE
236	1.754	1.754	Normal	STARE
239	1.770	1.728	Normal	STARE
240	1.762	1.762	Normal	STARE

Table 3. Average fractal dimension values for normal vs. abnormal fundus images

Diagnosis	Count	fd , ground truth
$\mu \pm \sigma$		
Normal	27	1.753 ± 0.0225
Abnormal	13	1.695 ± 0.0466

4.3 Analysis

Of the fundus images analyzed, those with retinal disease appear to have a lower fractal dimension than normal fundus images. We postulate the occlusion of vessel structures by disease features as the reason for this difference. With additional data and labels containing approximately equal representation of retinal diseases of interest, a systematic study of the viability of the fractal dimension as an indicator of retinal disease may be conducted. Results from such a study may drive the development of a retinal disease classifier using other metrics in addition to the fractal dimension such as the cup-to-disc ratio, a value currently used to detect glaucoma. A cup-to-disc ratio $> .6$ is considered to be suspicious for glaucoma [20]. The initial motivation for the use of fractal dimension as an indicator of diabetic retinopathy originates from the distinct loop-like patterns on the Hessian image of some images with diabetic retinopathy, as shown in Figure 7. These closed loop structures appear to contribute to a slightly lower fractal dimension than healthy fundus images, presumably because these loop-like features are localized to the affected regions of the eye. With additional data as well

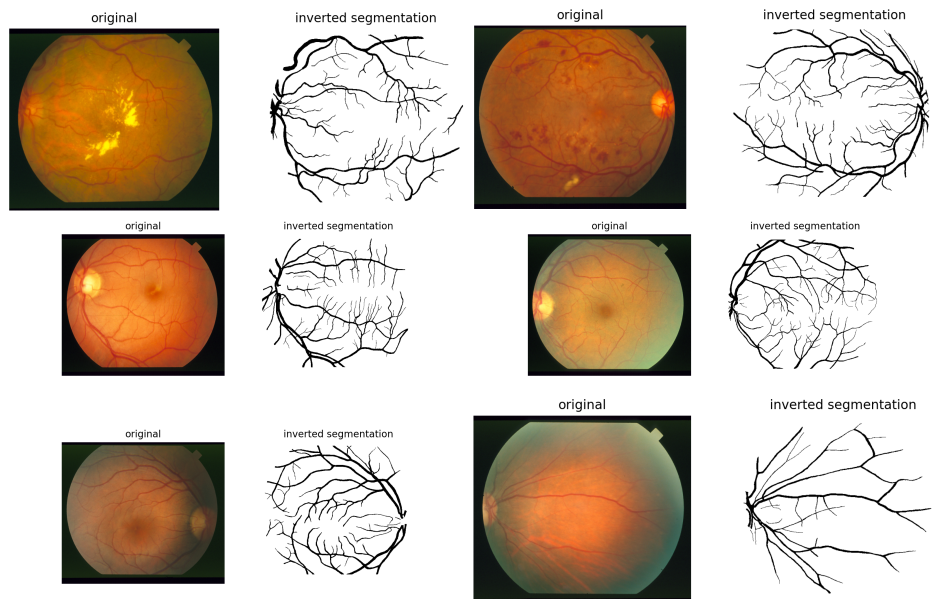


Fig. 9. 6 color fundus images and their inverted ground truth segmentations: STARE 001 (abnormal- background diabetic retinopathy), STARE 139 (abnormal- background diabetic retinopathy), STARE 236 (normal), STARE 239 (normal), STARE 240 (normal), STARE 291 (abnormal - vasculitis)

as a careful study of vessel structure changes over time with a disease such as diabetic retinopathy, the fractal dimension may supplement other existing measures to aid in automated diagnosis of fundus images. With a larger population of fractal dimension values for fundus images as well as corresponding diagnoses, certain values of the fractal dimension may give insight into the disease present in a fundus image, dependent on both the severity of the disease as well as the nature of the symptoms of the disease. As an example, symptoms of vasculitis (shown in the bottom right of Figure 9) include irritation of blood vessels which may be detected easily with the fractal dimension since irritated vessels may contain fewer vascular branches (and therefore less self-similarity), thus causing a notable decrease in the fractal dimension when compared to normal fundus images.

5 Code Usage

preprocess.py A pre-processing script to handle rgb to grayscale, multi-level Gaussian smoothing, and Hessian image extraction. The user should specify an input directory and output directory for the files as well as 3 sigmas values for smoothing, if applicable. The gray image of each input image is calculated by default. **Example usage:** ‘python preprocess.py input_dir output_dir s 1 2 4 a h’. **Example meaning:** for all images in input_dir, calculate the grayscale image, smooth with sigmas 1,2,4 and add the 3 images together, average the result, use this image to extract the Hessian image, and finally write the Hessian image to output_dir.

randomWalkSeg.py A utility to get the segmentation of the input images using the random walker algorithm. **Example usage:** ‘randomWalkSeg.py input_dir seg_dir v d > results.txt’. **Example meaning:** get the random walk segmentation for each file in input_dir, visualize each stage, and calculate Dice scores. Additionally, the output is redirected to results.txt. Option v visualizes each stage of the segmentation by opening a matplotlib figure containing the input Hessian image, the random walk result, and the cleaned final result. Intensity scaling, denoising, and small object removal are all completed internally. Option d lists the pairwise Dice scores between each of the following images: random walk result vs. input Hessian, ground truth vs. input Hessian, and random walk result vs. ground truth.

fractalDim.py A utility to calculate the fractal dimension for the input color image using its input segmentation image. Implements the counting boxes algorithm for covering an image in boxes and counting the boxes containing self-similarity detail over a range of scales. The fractal dimension is given by the log ratio of the number of boxes containing self-similarity detail, N , at scale r . **Example usage:** ‘python fractalDim.py seg_dir color_dir v d > results.txt’. **Example meaning:** get the fractal dimension for each file in seg_dir, visualize the result and write the fractal dimension values to results.txt

6 Conclusion

In this work we explore the difficulty of pre-processing fundus images for vessel segmentation. In particular, the nature of the vessel structures, heterogeneity of retinal features and orientation, and intensity variation all complicate pre-processing. We find that multi-level Gaussian smoothing of features is a useful step for enhancing vessel contrast, but does not generalize well to abnormal or diseased retinal anatomy. To handle this issue, we extract the Hessian image from the multi-level smoothed features and enhance it with intensity rescaling. The resulting image is the input to the random walk segmentation. We evaluate our success with Dice scores to compare our results with ground truth labels. We find that Dice scores for the random walk results compared to ground truth labels were higher than expected, and may be further improved with image-specific adjustment such as the minimum object size for small object removal and additional denoising for images with disease. Finally, we present fractal dimension values from the ground truth segmentation from the 40 total labeled images between the DRIVE and STARE datasets. This value may be a viable metric in a larger pipeline to determine whether a fundus image contains indicators of specific retinal disease. As shown in our results, the fractal dimension for the abnormal images studied are on average lower than the fractal dimension of normal images. We postulate this results from the occlusion of vessel structures reflected in the segmentation. Further work on labeled sets of fundus images are needed to assess the utility of the fractal dimension in categorizing eye disease, but this metric appears to be an appropriate value to quantify the "vesselness" of a fundus image. Overall, pre-processing of fundus images is complicated for a population of normal and abnormal fundus images because of the variety of disease symptoms and features as well as general vascular structure and intensity variation. We propose the enhanced Hessian image as input to the random walk segmentation algorithm and determine that the resulting Dice scores may be improved by case-specific or automated post-processing and enhancement. We find that the fractal dimension may be useful alongside a number of other feature classification metrics, such as the cup-to-disc ratio, in determining presence of disease in fundus images to ultimately improve diagnosis and retinal disease classification from fundus image segmentation results.

References

1. Jiang, Yun and Wang, Falin and Gao, Jing and Cao, Simin: Multi-Path Recurrent U-Net Segmentation of Retinal Fundus Image, *Applied Sciences* (2020)
2. Li, Yan and Gong, Haiming and Wu, Weilin and Liu, Gaoqiang and Chen, Guannan: An automated method using hessian matrix and random walks for retinal blood vessel segmentation (2015)
3. Z. Yan and X. Yang and K. -T. Cheng: A Three-Stage Deep Learning Model for Accurate Retinal Vessel Segmentation, *IEEE Journal of Biomedical and Health Informatics* (2015)

4. Hu, Qiao and Abràmoff, Michael D. and Garvin, Mona K: Automated Separation of Binary Overlapping Trees in Low-Contrast Color Retinal Image, Advanced Information Systems Engineering Lecture Notes in Computer Science (2013)
5. J.J. Staal AND M.D. Abramoff AND M. Niemeijer AND M.A. Viergever AND B. van Ginneken: Ridge based vessel segmentation in color images of the retina, IEEE Transactions on Medical Imaging (2004)
6. P. R. Wankhede and K. B. Khanchandani: Retinal Blood Vessel Segmentation in Fundus Images using Improved Graph Cut Method: 2018 International Conference on Smart Systems and Inventive Technology (ICSSIT) (2018)
7. Turbert, David: Fundus, American Academy of Ophthalmology (2020)
8. DOI: <https://www.opsweb.org/?page=fundusimaging>
9. Ophthalmoscopy, DOI: <https://www.hopkinsmedicine.org/wilmer/services/glaucoma/book/ch06s03.html>
10. Colomer, Adrián and Igual, Jorge and Naranjo, Valery: Detection of Early Signs of Diabetic Retinopathy Based on Textural and Morphological Information in Fundus Images, Sensors (Basel, Switzerland) (2020)
11. Hessian, from Wolfram MathWorld
12. Generalizing vesselness with respect to dimensionality and shape, Insight Journal (ISSN 2327-770X)
13. Morales, Jafet: Assessment of Iris Reflection Artifacts and Alignment in Fundus Images (2011)
14. Changlu Guo and Márton Szemenyei and Yugen Yi and Wenle Wang and Buer Chen and Changqi Fan: SA-UNet: Spatial Attention U-Net for Retinal Vessel Segmentation (2020)
15. DOI: <https://cecas.clemson.edu/ ahoover/stare/>
16. Fan Huang, Behdad Dashtbozorg, Jiong Zhang, Erik Bekkers, Samaneh Abbasi-Sureshjani, Tos T. J. M. Berendschot, Bart M. ter Haar Romeny, "Reliability of Using Retinal Vascular Fractal Dimension as a Biomarker in the Diabetic Retinopathy Detection", Journal of Ophthalmology, vol. 2016, Article ID 6259047, 13 pages, 2016. <https://doi.org/10.1155/2016/6259047>
17. L. Grady, "Random Walks for Image Segmentation," in IEEE Transactions on Pattern Analysis and Machine Intelligence, vol. 28, no. 11, pp. 1768-1783, Nov. 2006, doi: 10.1109/TPAMI.2006.233.
18. Otsu, Nobuyuki. "A threshold selection method from gray-level histograms." IEEE transactions on systems, man, and cybernetics 9.1 (1979): 62-66.
19. Jiaxin Wu, Xin Jin, Shuo Mi, Jinbo Tang. "An effective method to compute the box-counting dimension based on the mathematical definition and intervals" Results in Engineering (2020)
20. Español, Informacion en, et al. "Optic Nerve Cupping." Glaucoma Research Foundation, <https://www.glaucoma.org/glaucoma/optic-nerve-cupping.php>. Accessed 9 Dec. 2020.